Article

Discovery Medicine 2025; 37(198): 1399–1408
https://doi.org/10.24976/Discov.Med.202537198.121

High-Cholesterol Diet Induces Dyslipidemia, Inflammation, Plaque Instability, and Vascular Remodeling in ApoE$^{-/-}$ and Wild-Type Mice

Wenrong Wang[1,2,3,†], Yaozhi Qi[4,†], Pingjuan Ni[1,2,5], Chen Cheng[6], Yanan Chen[3], Jie Lu[3], Pinjing Hui[1,2,*]

[1]Department of Neurosurgery, The First Affiliated Hospital of Soochow University, 215031 Suzhou, Jiangsu, China
[2]Department of Stroke Center, The First Affiliated Hospital of Soochow University, 215031 Suzhou, Jiangsu, China
[3]Department of Ultrasound, Lianyungang Maternal and Child Health Hospital, 222000 Lianyungang, Jiangsu, China
[4]Department of Laboratory, Lianyungang Maternal and Child Health Hospital, 222000 Lianyungang, Jiangsu, China
[5]Department of Ultrasound, The Second Hospital of Shandong University, 250033 Jinan, Shandong, China
[6]Department of Ultrasound, Lianyungang Traditional Chinese Medicine Hospital, 222004 Lianyungang, Jiangsu, China
*Correspondence: pinjing-hui@163.com (Pinjing Hui)
[†]These authors contributed equally.
Published: 20 July 2025

Background: Atherosclerosis (AS) is a primary driver of cardiovascular disease. This study aimed to investigate the effects of a high-cholesterol diet (HD) on body weight, lipid profile, inflammatory cytokines, plaque stability, and histopathological changes in Apolipoprotein E (ApoE)$^{-/-}$ and wild-type (WT) mice, to clarify the underlying mechanisms of AS.

Methods: ApoE$^{-/-}$ and wild-type mice were fed HD or normal diet (ND) for 4 weeks. Body weight was monitored weekly to assess the development of obesity. The serum levels of blood lipids and inflammatory factors were examined using the corresponding kits. The expression of plaque stability markers was confirmed using quantitative reverse-transcription polymerase chain reaction (qRT-PCR) and Western blot. Besides, the structure and fat deposition of coronary artery tissues were assessed using hematoxylin and eosin (H&E), Masson trichrome, oil red O, Prussian blue, and immunohistochemical staining.

Results: Relative to the ND group, the body weight of mice notably increased in the HD group ($p < 0.01$). HD feeding elevated serum lipids and pro-inflammatory markers in ApoE$^{-/-}$ and wild-type mice ($p < 0.01$). Expression of plaque instability markers was significantly upregulated in HD-fed groups ($p < 0.05$). Histological analysis revealed structural disorganization, increased lipid and iron deposition, and greater collagen accumulation in coronary tissues, particularly in the ApoE$^{-/-}$ mice.

Conclusion: This study demonstrated that HD might accelerate AS by promoting obesity, dyslipidemia, inflammation, plaque instability, and vascular remodeling, especially in genetically susceptible ApoE$^{-/-}$ mice. These results may provide new insights for AS prevention and therapy.

Keywords: high-cholesterol diet; atherosclerosis; lipid metabolism; plaque instability; vascular remodeling; ApoE$^{-/-}$ mice

Introduction

Atherosclerosis (AS) is a primary driver of cardiovascular disease (CVD), characterized by lipid deposition in arterial walls [1], activation of inflammatory pathways [2], and remodeling of vascular structures [3]. As lipids accumulate within the vessel wall, arteries are subject to progressive narrowing and loss of flexibility, resulting in the formation of atherosclerotic plaques [4]. Over time, these plaques become increasingly unstable, making them prone to rupture and thrombosis, which can further obstruct blood flow and lead to severe complications, such as myocardial infarction and stroke [5]. The development and progression of AS involve multiple interconnected processes, including dyslipidemia, inflammatory responses, plaque instability, and vascular remodeling [6,7]. These mechanisms interact dynamically, accelerating vascular dysfunction; such concerted processes underscore the need for systematic studies to elucidate their contributions, which are essential for understanding AS pathogenesis and advancing early diagnostic tools and precise therapeutic strategies.

High-cholesterol diet (HD) is widely employed as an experimental model to replicate the dyslipidemic state observed in humans with AS [8,9]. Previous studies have demonstrated that HD increases serum total cholesterol (TC), low-density lipoprotein cholesterol (LDL-C), and triacylglycerol (TG) levels, while simultaneously reducing high-density lipoprotein cholesterol (HDL-C), resulting in a marked disruption of lipid homeostasis [8–10]. This dyslipidemic state not only promotes cholesterol deposition

in the arterial wall but also triggers local immune activation, leading to the release of inflammatory mediators [11]. These inflammatory responses amplify endothelial damage and accelerate plaque formation and progression [12]. Moreover, HD induces oxidative stress and promotes the migration and proliferation of smooth muscle cells, contributing to vascular fibrosis and remodeling, which further destabilizes plaques and increases the risk of rupture and thrombosis [13]. Together, these pathological changes demonstrate that HD serves not only as a critical factor driving AS progression but also as a valuable tool for investigating its underlying mechanisms. This diet-induced model enables researchers to explore the intricate relationships among dyslipidemia, inflammation, plaque stability, and vascular remodeling.

Apolipoprotein E (ApoE) is an essential protein involved in lipid metabolism, facilitating the clearance of circulating cholesterol [14]. Mice deficient in ApoE ($ApoE^{-/-}$ mice) are widely recognized as a robust animal model for studying AS because their inability to efficiently clear LDL-C results in severe hyperlipidemia and increased lipid deposition in arterial walls [15]. These mice exhibit many pathological features similar to human AS, including dyslipidemia, inflammation, and plaque instability, making them an ideal model for investigating the mechanisms underlying AS [16]. Moreover, $ApoE^{-/-}$ mice fed an HD develop atherosclerotic plaques rapidly and consistently, providing a reliable platform to study lipid metabolism, inflammatory processes, and vascular remodeling under controlled conditions. This makes $ApoE^{-/-}$ mice particularly suitable for studying the effects of HD on AS progression, as they exhibit more severe and accelerated atherosclerotic changes due to their impaired ability to clear cholesterol.

Despite significant progress in AS research, much of the focus has been placed on individual pathological processes such as dyslipidemia or inflammation. However, a more integrated approach that examines how HD affects multiple facets of AS, such as lipid metabolism, inflammatory responses, plaque stability, and vascular remodeling, has been relatively underexplored. Furthermore, while $ApoE^{-/-}$ mice are extensively used to study AS, there remains a lack of studies that systematically compare the pathological effects of HD-induced AS in both $ApoE^{-/-}$ and C57BL/6 wild-type mice. This highlights the gap in the current literature, as a systematic comparison of the atherosclerotic pathology between these two mouse strains under HD conditions is still lacking.

In this study, we hypothesize that $ApoE^{-/-}$ mice will exhibit more severe atherosclerotic pathology, including greater lipid accumulation, inflammation, plaque instability, and vascular remodeling, compared to wild-type mice when fed an HD. By comparing these two models, we aim to elucidate the complex and dynamic mechanisms driving the progression of AS and provide a clearer understanding of how HD influences the multifactorial nature of AS.

Materials and Methods

Animals

Wild-type (n = 16, each weighing 20 ± 2 g) and $ApoE^{-/-}$ C57BL/6J mice (n = 16, each weighing 25 ± 2 g) (male, aged 8–10 weeks) were obtained from Beijing Vital River Laboratory Animal Technology Co., Ltd. (Beijing, China). Mice were housed in a controlled environment with temperature set at 19–23 °C and humidity at 32%–55%, under a 12-h light/dark cycle. The mice were given free access to food and water. All animal experiments were approved by the Institutional Animal Care and Use Committee of The First Affiliated Hospital of Soochow University. Before the start of the experiment, all mice were adaptively fed with an ordinary diet for 1 week.

Experimental Design and Sample Collection

Following a one-week acclimatization period with normal diet (ND), the mice were randomly assigned to four groups (n = 8 per group) and blinding was applied during both data collection and data analysis to minimize bias. The groups included: $ApoE^{-/-}$ ND group ($ApoE^{-/-}$ mice fed an ND), $ApoE^{-/-}$ HD group ($ApoE^{-/-}$ mice fed an HD), ND group (C57BL/6J wild-type mice fed an ND), and HD group (C57BL/6J wild-type mice fed an HD). The ND consisted of 10% fat, 20% protein, and 70% carbohydrate, while the HD contained 40% fat (including 1% cholesterol), 20% protein, and 40% carbohydrate. The experimental duration was 20 weeks. Body weight was measured weekly for the first 4 weeks using an electronic scale (SECURA26-1S, Sartorius, Göttingen, Germany), as an early indicator of diet-induced metabolic alterations. Early-phase body weight changes were emphasized to capture the onset of obesity-related responses, which typically precede measurable histopathological and inflammatory changes.

At the end of the 20-week feeding period, the mice were fasted for 12 h, with water provided *ad libitum*. Blood collection was performed under 2% isoflurane inhalation anesthesia, with blood drawn from the inner canthus into sterile centrifuge tubes. The samples were centrifuged at 3000 $\times g$ for 15 min at 4 °C, and serum was aliquoted into 20 µL portions and stored at –80 °C for future analysis.

After blood collection, the mice were humanely euthanized by CO_2 asphyxiation in accordance with institutional animal care guidelines. Vascular perfusion was carried out using cold saline (0.9% NaCl) injected into the left ventricle, with effluent collected from the right atrium to ensure the removal of residual blood. Following perfusion, the heart, aorta, and carotid arteries were carefully excised, with tissue from the aortic root near the heart base specifically collected for histological analysis.

Serum Lipid Measurement

Serum levels of TC, TG, LDL-C, and HDL-C were determined using commercially available kits based on man-

ufacturers' instructions. Serum samples from 6 mice per group, which were selected based on volume adequacy and absence of hemolysis, were used for analysis. The kits included TC Content Assay Kit (AKFA002M, Boxbio, Beijing, China), TG Content Assay Kit (AKFA003M, Boxbio, China), LDL/very-low-density lipoprotein cholesterol (VLDL-C) Content Assay Kit (AKBL012M, Boxbio, China), and HDL-C Content Assay Kit (AKBL011M, Boxbio, China). The measurements were performed using a microplate reader (Varioskan ALF, Thermo Fisher, Waltham, MA, USA) with wavelengths set at 500 nm for TC, 420 nm for TG, and 550 nm for LDL-C and HDL-C. The concentration of each lipid component was determined by comparing the absorbance to a standard curve generated using known concentrations of the lipid standards provided in the kits.

Enzyme-Linked Immunosorbent Assay

Levels of interleukin (IL)-6, IL-1β, IL-18, C-reactive protein (CRP), tumor necrosis factor alpha (TNF-α), and soluble intercellular adhesion molecule 1 (sICAM-1) in the serum were quantified by means of enzyme-linked immunosorbent assay (ELISA) kits according to the manufacturer's protocols. The kits included mouse IL-6 ELISA Kit (PI326, Beyotime, Shanghai, China), mouse IL-18 ELISA Kit (PI553, Beyotime, China), mouse CRP ELISA Kit (PC186, Beyotime, China), mouse TNF-α ELISA Kit (PT512, Beyotime, China), mouse IL-1β ELISA Kit (E-EL-M0037, Elabscience, Wuhan, China), and mouse sICAM-1 ELISA Kit (ml037656, Mlbio, Shanghai, China). Absorbance was measured using a microplate reader (Varioskan ALF, Thermo Fisher, Waltham, MA, USA) at a wavelength of 450 nm. Serum samples from six mice per group were used, based on volume sufficiency and absence of hemolysis.

Quantitative Reverse-Transcription Polymerase Chain Reaction

Total RNA was extracted from the aortic tissues using the Tissue Total RNA Isolation Kit V2 (RC112, Vazyme, Nanjing, China). RNA was assessed with a NanoDrop spectrophotometer (ND-8000-GL, Thermo Fisher, Waltham, MA, USA). cDNA was synthesized using the HiScript III 1st Strand cDNA Synthesis Kit (R312, Vazyme, China). Quantitative reverse-transcription polymerase chain reaction (qRT-PCR) was performed using Taq Pro Universal SYBR qPCR Master Mix (Q712, Vazyme, China) on a CFX96 Touch Real-Time PCR System (Bio-Rad, Hercules, CA, USA). The relative expression of target genes was normalized to that of glyceraldehyde-3-phosphate dehydrogenase (GAPDH), and fold changes were calculated using the $2^{-\Delta\Delta Ct}$ method. Primer sequences are listed in Table 1.

Table 1. Primer sequences.

Gene	Sequences (5′ to 3′)
PTX3	Forward: GGCCGAGAACTCGGATGATT
	Reverse: AGCATGCGCTCTCTCATCTG
PLA2G7	Forward: TCACAAGACTCCAATCGG TCAG
	Reverse: CGACGGGGTACGATCCATTTC
FGF23	Forward: TAGAGCCTATTCAGACACTTC
	Reverse: CATCAGGGCACTGTAGATAG
MMP-9	Forward: TTCTGGCACACGCCTTTC
	Reverse: CCATAGTAAGTGGGGATCACG
ICAM-1	Forward: CCTCAGCCTCGCTATGGCT
	Reverse: CCGAGCAGGACCAGGAGT
VCAM-1	Forward: GCAAGTCTACATATCACCCAAG
	Reverse: GCAAGTCTACATATCACCCAAG
GAPDH	Forward: CAGGTTGTCTCCTGCGACTT
	Reverse: TATGGGGGTCTGGGATGGAA

PTX3, pentraxin 3; *PLA2G7*, phospholipase A2 group VII; *FGF23*, fibroblast growth factor 23; *MMP-9*, matrix metallopeptidase 9; *ICAM-1*, intercellular adhesion molecule 1; *VCAM-1*, vascular cell adhesion molecule 1; *GAPDH*, glyceraldehyde-3-phosphate dehydrogenase.

Western Blotting

Aortic tissues were homogenized in radioimmunoprecipitation assay (RIPA) buffer supplemented with phenylmethylsulfonyl fluoride (PMSF) (ST506, Beyotime, China). After quantification using the bicinchoninic acid (BCA) Protein Assay Kit (P0012S, Beyotime, China), 30 µg of proteins were denatured and separated on a 10% sodium dodecyl sulfate-polyacrylamide gel electrophoresis (SDS-PAGE) gel (Biosharp, Hefei, China) and transferred to polyvinylidene difluoride (PVDF) membranes (SLBN00010B, Merck Millipore, Burlington, MA, USA). Membranes were blocked with 5% non-fat milk (BioFroxx, China) in Tris-buffered saline (TBS; Biosharp, China) for 1 h and incubated overnight at 4 °C with primary antibodies: anti-pentraxin 3 (PTX3) (1:1000, ab125007, Abcam, Cambridge, UK), anti-phospholipase A2 group VII (PLA2G7) (1:1000, A24499, ABclonal, Wuhan, China), anti-fibroblast growth factor 23 (FGF23) (1:1000, A25006, ABclonal, Wuhan, China), anti-matrix metallopeptidase 9 (MMP-9) (1:1000, 82854-1-RR, Proteintech, Rosemont, IL, USA), anti-ICAM-1 (1:1000, ab109361, Abcam, Cambridge, UK), and anti-vascular cell adhesion molecule 1 (VCAM-1) (1:1000, ab134047, Abcam, Cambridge, UK). Membranes were then washed and incubated with horseradish peroxidase (HRP)-conjugated secondary antibodies (1:5000, bs-0295G, Bioss, Woburn, MA, USA). GAPDH (1:2500, ab9485, Abcam, Cambridge, UK) was used as an internal control to ensure equal protein loading. Protein bands were visualized using the enhanced chemiluminescence (ECL) detection system (NCM Biotech, Suzhou, China, P2100) and analyzed with ImageJ version 1.53 software (National Institutes of Health, Bethesda, MD, USA).

Hematoxylin and Eosin (H&E) Staining

Following the euthanization of the animals, their heart and aorta tissues were carefully excised and immediately fixed in 4% paraformaldehyde (AR1069, Beijing Bozhide, Beijing, China) for 24 h. Subsequently, the tissues were dehydrated in a graded ethanol series, cleared with xylene, and embedded in paraffin blocks. Sections (5 µm) were deparaffinized with xylene, rehydrated, and stained with hematoxylin and eosin using a commercially available kit (C0105M, Beyotime, China). After dehydration, clearing with xylene, and mounting with a coverslip, the stained sections were observed under a light microscope (Olympus CX23, Olympus, Tokyo, Japan).

Oil Red O Staining

After euthanasia, aorta samples were isolated from the mice and fixed in 4% paraformaldehyde for 24 h. Following fixation, the aorta was washed three times. Then, the aorta was longitudinally opened along its vessel wall to allow efficient staining of lipid deposits. The aorta was immersed in oil red O staining solution (G1260, Solarbio, Beijing, China) for 60 min at 37 °C. After staining, the vessel was differentiated in 75% ethanol until lipid deposits. After washing, the stained tissue was photographed. For sectioning, the sections were fixed for 10 min, followed by washing. The sections were dehydrated using 60% isopropanol for 5 min and incubated with oil red O staining solution (Solarbio, China) for 10 min. After staining, the sections were differentiated using 60% isopropanol, washed, counterstained with hematoxylin for 3–5 min, washed, dehydrated, cleared in xylene, and mounted with glycerol gelatin (G8590, Solarbio, China). The sections were examined using a light microscope (Olympus CX23, Olympus, Tokyo, Japan). Quantification of lipid area percentage from the oil red O staining was performed using ImageJ software.

Masson Trichrome Staining

Collagen deposition was assessed using the Masson Trichrome Staining Kit (G1340, Solarbio, China) following the manufacturer's protocol. Briefly, tissue sections (5 µm) were deparaffinized with xylene and rehydrated through graded ethanol. The sections were stained with Weigert's iron hematoxylin solution for 10 min to stain the nuclei. After washing, the sections were incubated with Ponceau S for 10 min to stain collagen fibers red. Next, the sections were treated with phosphomolybdic acid solution for 5 min, followed by staining with aniline blue solution for 15 min to stain collagen fibers blue. The sections were then dehydrated, cleared with xylene, and mounted with glycerol gelatin. Stained sections were observed under a light microscope (Olympus CX23, Olympus, Tokyo, Japan). Quantification of collagen content was performed by measuring the area of collagen fibers in the tissue sections using ImageJ software. The collagen area percentage was calculated relative to the total tissue area.

Prussian Blue Staining

Iron deposits were examined using a Prussian Blue staining kit (G1029, Solarbio, China) following the manufacturer's instructions. Tissue sections (5 µm) were deparaffinized with xylene and rehydrated through graded ethanol. The sections were incubated in potassium ferrocyanide solution for 30 min, followed by washing in distilled water. After incubation, the sections were counterstained with nuclear fast red for 10 min to stain the nuclei. The sections were then dehydrated, cleared with xylene, and mounted with glycerol gelatin. Stained sections were observed under a light microscope (Olympus CX23, Olympus, Tokyo, Japan).

Immunohistochemistry Assay

After deparaffinization and antigen retrieval, the sections were treated with 3% hydrogen peroxide for 10 min, incubated with 5% bovine serum albumin for 20 min and anti-potassium channel interacting protein 2 (KChIP2) (1:100, ab252539, Abcam, Cambridge, UK) overnight at 4 °C. Subsequently, the sections were incubated with a secondary antibody (1:200, ab150113, Abcam, Cambridge, UK) for 1 h after washing. The sections were then developed using 3,3′-diaminobenzidine (DAB) substrate (Sigma-Aldrich, St. Louis, MO, USA) for visualization, and images were captured using a light microscope (Olympus CX23, Olympus, Tokyo, Japan). KChIP2 expression was quantified as the integrated optical density (IOD) of DAB staining, normalized to the ApoE$^{-/-}$ ND group (set as 1.00 $\pm$ standard deviation (SD)) for cross-group comparison.

Statistical Analysis

Data are expressed as means $\pm$ SD from three independent replicates. Statistical analysis and graphing were performed using GraphPad Prism 9 (version 9.4.0; GraphPad Software Inc., San Diego, CA, USA). For comparing differences between groups, one-way analysis of variance (ANOVA) followed by Tukey's post-hoc test was applied, and $p < 0.05$ was considered statistically significant.

Results

HD Induces Obesity and Alters Lipid Metabolism in ApoE$^{-/-}$ and Wild-Type Mice

To evaluate the effect of HD on obesity, the body weight of both ApoE$^{-/-}$ and wild-type mice was monitored weekly for 4 weeks. As shown in Fig. 1A, both ApoE$^{-/-}$ and wild-type mice fed an HD exhibited a progressive increase in body weight over the 4-week period compared to their ND-fed counterparts ($p < 0.01$). Under the same dietary conditions, the body weight of ApoE$^{-/-}$ mice was significantly higher than that of wild-type mice ($p < 0.001$), suggesting that both genotype and diet contributed to obesity susceptibility.

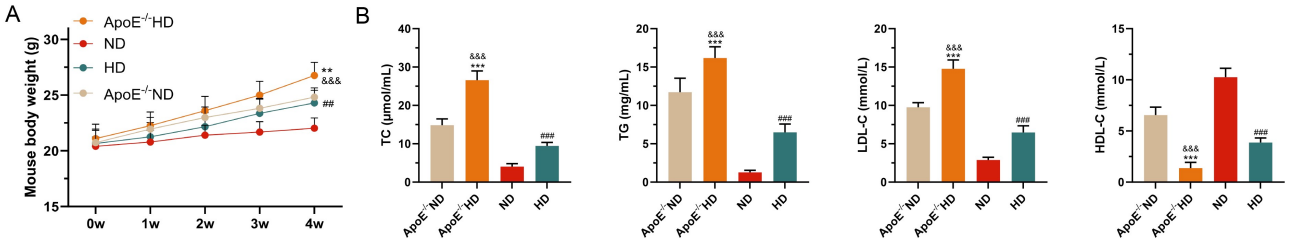

Fig. 1. Effects of HD on body weight and serum lipid profile in ApoE$^{-/-}$ and wild-type mice. (A) The body weight of ApoE$^{-/-}$ and wild-type mice fed an ND or an HD was measured weekly for 4 weeks using an electronic scale ($n = 8$). (B) The serum levels of TC, TG, LDL-C, and HDL-C in ApoE$^{-/-}$ and wild-type mice fed an ND or an HD were quantitatively assessed using biochemical assay kits ($n = 6$). Data are expressed as mean ± standard deviation (SD). Statistical comparisons were performed using one-way ANOVA with Tukey's post-hoc test. $^{**}p < 0.01$, $^{***}p < 0.001$ vs. ApoE$^{-/-}$ND; $^{\#\#}p < 0.01$, $^{\#\#\#}p < 0.001$ vs. ND; $^{\&\&\&}p < 0.001$ vs. HD. Abbreviations: ANOVA, analysis of variance; ApoE, apolipoprotein e; HD, high-cholesterol diet; HDL-C, high-density lipoprotein cholesterol; LDL-C, low-density lipoprotein cholesterol; ND, normal diet; TC, total cholesterol; TG, triacylglycerol.

To investigate changes in lipid metabolism, the serum levels of TG, TC, LDL-C, and HDL-C were measured (Fig. 1B). In animals of both genotypes, HD feeding markedly elevated the levels of TC, TG, and LDL-C, while HDL-C levels showed a significant decline ($p < 0.001$). Moreover, the ApoE$^{-/-}$ mice displayed higher TC, TG, and LDL-C levels and lower HDL-C levels than the wild-type mice under HD conditions ($p < 0.001$), indicating a more severe lipid disorder in the ApoE-deficient context.

These findings indicated that HD induces dyslipidemia and exacerbates obesity, especially in genetically susceptible ApoE$^{-/-}$ mice.

HD Exacerbates Systemic Inflammation and Impairs Plaque Stability in ApoE$^{-/-}$ and Wild-Type Mice

To investigate the pro-inflammatory effects of HD, we assessed serum inflammatory cytokine levels in ApoE$^{-/-}$ and wild-type mice. As shown in Fig. 2A, HD-fed mice exhibited significantly elevated levels of IL-6, IL-1β, IL-18, CRP, TNF-α, and sICAM-1 compared to their ND-fed counterparts ($p < 0.001$). These values were higher in HD-fed ApoE$^{-/-}$ mice than in HD-fed wild-type mice ($p < 0.001$), suggesting a synergistic effect of genetic susceptibility and dietary challenge on systemic inflammation.

To further assess plaque stability, we measured the mRNA and protein expression of instability-associated markers in aortic tissues. The qRT-PCR results (Fig. 2B) revealed significant upregulation of PTX3, PLA2G7, FGF23, MMP-9, ICAM-1, and VCAM-1 in HD-fed groups ($p < 0.01$). Consistent with the transcriptomic data, Western blot analysis (Fig. 2C) showed elevated protein expression levels of the same markers ($p < 0.05$). Compared with HD-fed wild-type mice, ApoE$^{-/-}$ mice that were fed an HD diet displayed significantly higher levels of both inflammatory cytokines and plaque instability markers ($p < 0.01$), indicating that ApoE deficiency markedly amplified the detrimental effects of HD on vascular health.

These findings collectively indicated that HD enhanced systemic inflammation and reduced plaque stability in animals of both genotypes, with a more severe response observed in ApoE$^{-/-}$ mice.

HD Induces Vascular Structural Remodeling and Lipid Deposition in ApoE$^{-/-}$ and Wild-Type Mice

To assess the impact of an HD on coronary artery structure, we performed histological staining of coronary artery tissues. H&E staining showed that the coronary arteries of ND-fed ApoE$^{-/-}$ and wild-type mice exhibited well-organized architecture, with thin vessel walls and uniformly arranged smooth muscle cells (Fig. 3A). In contrast, HD-fed mice revealed pronounced vascular disorganization and thickened vessel walls, especially in ApoE$^{-/-}$ mice, indicating more severe structural remodeling.

Masson trichrome staining revealed minimal collagen deposition in the coronary arteries of ND-fed groups, while extensive collagen accumulation was observed in HD-fed mice ($p < 0.05$), with the ApoE$^{-/-}$ HD group displaying the highest percentage of collagen-positive area ($p < 0.01$) (Fig. 3B). These results indicated that HD promotes vascular fibrosis, which is more severe in genetically susceptible mice.

Macroscopic oil red O staining of the aorta demonstrated minimal lipid accumulation in the ND groups. In contrast, HD-fed mice showed substantial lipid deposition along the aortic wall, which was more extensive in ApoE$^{-/-}$ mice compared to wild-type mice (Fig. 3C). Moreover, sectional oil red O staining of coronary artery sections showed similar trends: HD-fed ApoE$^{-/-}$ mice exhibited significantly larger lipid-laden areas than the other groups ($p < 0.001$) (Fig. 3D).

Together, these findings confirmed that HD induced significant lipid accumulation and extracellular matrix remodeling in the vascular system, with ApoE deficiency amplifying these pathological changes.

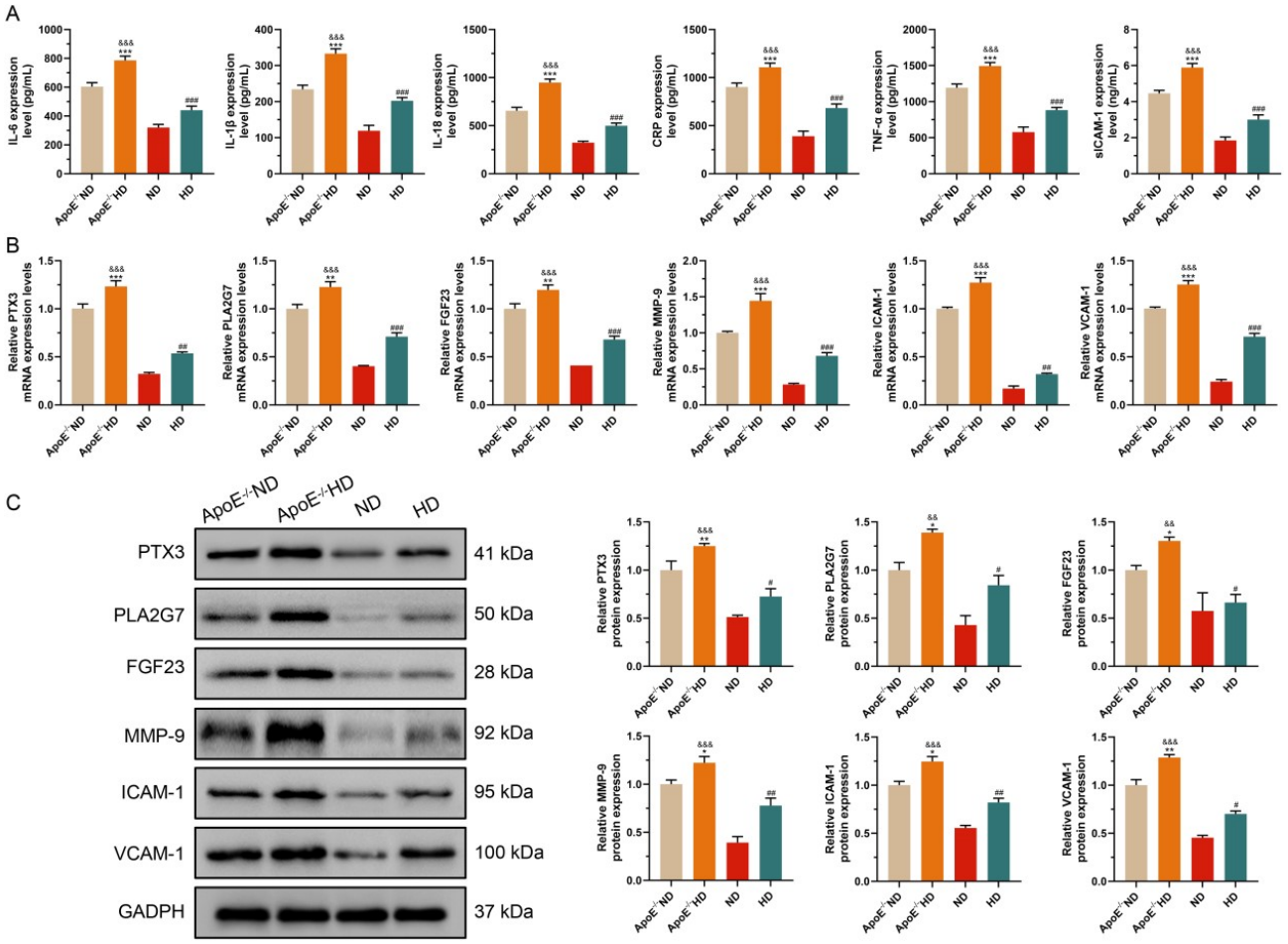

Fig. 2. Serum inflammatory cytokines and plaque stability markers. (A) Serum levels of IL-6, IL-1β, IL-18, CRP, TNF-α, and sICAM-1 were measured using ELISA kits in ApoE$^{-/-}$ and wild-type mice after feeding with ND or HD ($n = 6$). (B) mRNA expression levels of PTX3, PLA2G7, FGF23, MMP-9, ICAM-1, and VCAM-1 were analyzed in aortic tissues by qRT-PCR. (C) Protein levels of PTX3, PLA2G7, FGF23, MMP-9, ICAM-1, and VCAM-1 were assessed in aortic tissues by means of Western blotting. Data are expressed as means $\pm$ SD ($n = 3$). Statistical comparisons were performed using one-way ANOVA with Tukey's post-hoc test. $^{*}p < 0.05$, $^{**}p < 0.01$, $^{***}p < 0.001$ vs. ApoE$^{-/-}$ND; $^{\#}p < 0.05$, $^{\#\#}p < 0.01$, $^{\#\#\#}p < 0.001$ vs. ND; $^{\&\&}p < 0.01$, $^{\&\&\&}p < 0.001$ vs. HD. Abbreviations: ANOVA, Analysis of variance; CRP, C-reactive protein; HD, High-cholesterol diet; IL, Interleukin; ND, Normal diet; qRT-PCR, quantitative reverse-transcription polymerase chain reaction; sICAM-1, Soluble intercellular adhesion molecule 1; TNF-α, Tumor necrosis factor alpha.

HD Promotes Coronary Iron Deposition and Upregulates KChIP2 Expression in ApoE$^{-/-}$ and Wild-Type Mice

To further explore the pathological consequences of HD on the cardiovascular system, we assessed iron deposition and KChIP2 protein expression in coronary artery tissues.

Prussian blue staining revealed negligible iron accumulation in the ND-fed ApoE$^{-/-}$ and wild-type mice. In contrast, marked iron deposition was observed in the coronary vessels of HD-fed ApoE$^{-/-}$ mice, while only mild or sparse deposition was noted in the HD group (Fig. 4A).

To assess myocardial remodeling, we analyzed the expression of KChIP2, a potassium channel-interacting protein implicated in cardiac excitability and remodeling. Immunohistochemical staining demonstrated weak KChIP2 expression in ND-fed animals of both genotypes. However, HD feeding significantly increased KChIP2 expression in coronary arteries ($p < 0.001$), with the strongest staining observed in the ApoE$^{-/-}$ HD group ($p < 0.001$) (Fig. 4B).

Together, these data indicated that HD induced iron accumulation and upregulated myocardial remodeling markers, particularly in ApoE$^{-/-}$ mice.

Discussion

The onset and progression of AS involve multiple complex pathological mechanisms, including dyslipidemia, inflammation, plaque instability, and vascular remodeling

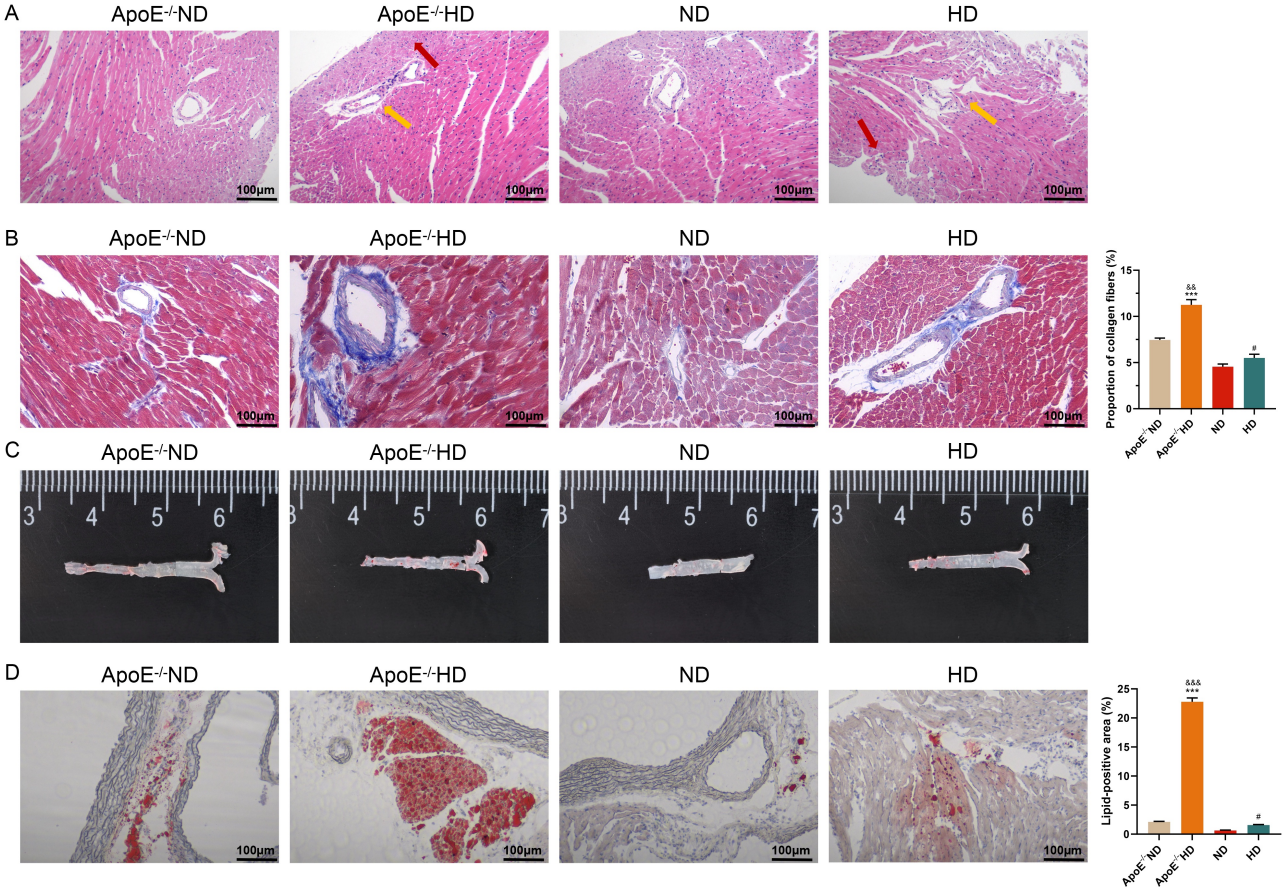

Fig. 3. Histological analysis of coronary artery tissues. (A) The morphology of coronary artery tissues from ND- or HD-fed ApoE$^{-/-}$ and wild-type mice was evaluated using H&E staining. Scale bar = 100 μm. Red arrows indicate regions of thickened vessel walls, and yellow arrows denote vascular disorganization. (B) Collagen fibers in the coronary artery tissues of mice were visualized by means of Masson trichrome staining. Scale bar = 100 μm. (C) Oil red O staining of lipid deposition in aortic tissues. (D) The lipid droplets in coronary artery sections were visualized using oil red O staining. Scale bar = 100 μm. Data are expressed as means ± SD (n = 3). Statistical comparisons were performed using one-way ANOVA with Tukey's post-hoc test. ***$p < 0.001$ vs. ApoE$^{-/-}$ND; $^{\#}p < 0.05$ vs. ND; $^{\&\&}p < 0.01$, $^{\&\&\&}p < 0.001$ vs. HD. Abbreviations: ANOVA, Analysis of variance; HD, High-cholesterol diet; ND, Normal diet.

[17,18]. As a widely used method for inducing AS in animal models, HD exerts its effects through the disruption of lipid metabolism and induction of inflammatory and structural vascular changes [19]. In this study, HD significantly elevated serum TC, LDL-C, and TG levels, while decreasing HDL-C, consistent with previous findings [20,21]. These lipid disturbances accelerate cholesterol deposition in the arterial wall, contributing to the initiation of plaque formation [22–24].

Inflammation is a central driver of AS progression [25,26], as evidenced by the elevated levels of inflammatory markers (such as IL-6, IL-1β, TNF-α, and CRP) in the serum of HD-fed mice. These markers enhance endothelial permeability, facilitating lipid and monocyte infiltration, which further promotes plaque instability [27–29]. This study found that HD significantly upregulated key markers associated with plaque instability, such as MMP-9 and PTX3. These markers play pivotal roles in extracellular matrix degradation and inflammatory cell infiltration, which compromise the structural integrity of plaques and make them more prone to rupture [30–33]. Therefore, these findings provide valuable insights into the molecular mechanisms of plaque instability, highlighting potential targets for therapeutic intervention.

Vascular remodeling, which includes smooth muscle cell migration, proliferation, and extracellular matrix remodeling, is another critical feature of AS [34,35]. This process is enhanced by HD, as evidenced by increased collagen deposition in the arterial wall, which was confirmed by Masson trichrome staining. Importantly, the increased expression of MMP-9 may facilitate extracellular matrix degradation, triggering compensatory collagen deposition as part of a maladaptive vascular remodeling process, ultimately contributing to vascular fibrosis and stiffness [30]. These changes, induced by HD, may contribute to the structural disorganization of the vascular wall and the desta-

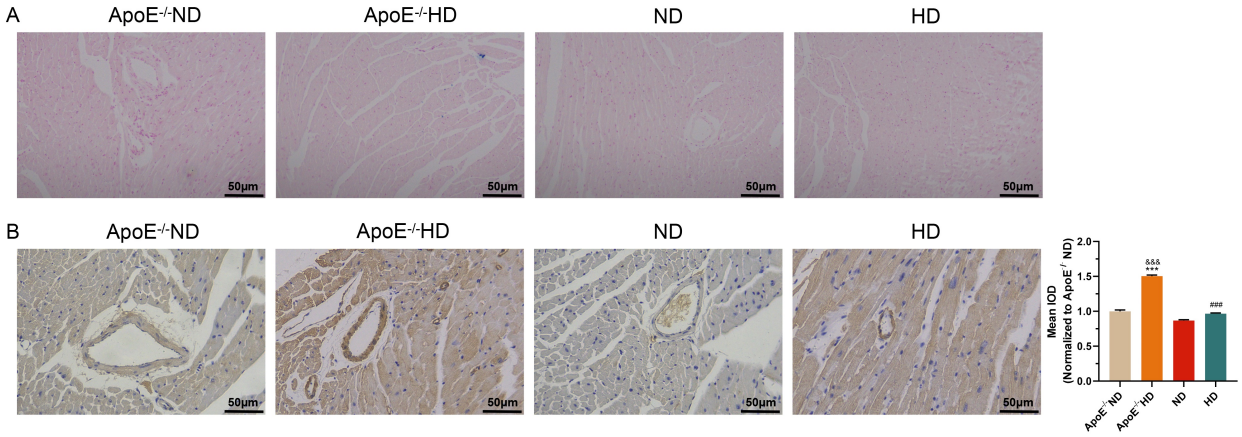

Fig. 4. Iron deposition and KChIP2 protein expression in coronary artery tissues. (A) Prussian blue staining showing iron deposition in coronary artery tissues of ND- or HD-fed ApoE$^{-/-}$ and wild-type mice. Scale bar = 50 μm. (B) Immunohistochemical staining of KChIP2 protein expression in the coronary artery tissues of mice. Scale bar = 50 μm. Data are expressed as mean ± SD ($n = 3$). Statistical comparisons were performed using one-way ANOVA with Tukey's post-hoc test. ***$p < 0.001$ vs. ApoE$^{-/-}$ND; $^{\#\#\#}p < 0.001$ vs. ND; $^{\&\&\&}p < 0.001$ vs. HD. Abbreviations: ANOVA, Analysis of variance; HD, High-cholesterol diet; ND, Normal diet.

bilization of atherosclerotic plaques [36]. Our study also highlights the role of iron deposition in AS progression. Increased iron accumulation, as shown by Prussian blue staining, may promote oxidative stress and exacerbate inflammatory responses, further accelerating vascular damage and plaque instability [37–39].

Additionally, we observed an increase in KChIP2 expression in HD-fed mice. While KChIP2 is not a conventional marker for AS, it has been implicated in the regulation of vascular tone and endothelial function [40]. KChIP2 is known to be involved in modulating the electrical activity of vascular smooth muscle cells and endothelial cells, influencing vascular tone and response to hemodynamic stress. Altered KChIP2 expression could influence the mechanical properties and inflammatory profile of the vascular wall, suggesting its potential role in AS progression. Its upregulation in the HD group may represent an adaptive response to altered vascular function or stress. Further investigation into KChIP2's involvement in atherosclerotic vascular remodeling is warranted to determine its precise role in plaque stability and the progression of AS.

In terms of model comparison, ApoE$^{-/-}$ mice on HD displayed more pronounced pathological changes compared to wild-type mice, underscoring the impact of ApoE deficiency in amplifying the effects of HD. ApoE$^{-/-}$ mice, which are prone to severe lipid accumulation and plaque formation, serve as a useful model for studying the advanced stages of AS [15]. In contrast, wild-type mice on HD exhibit milder forms of AS, which potentially represent early-stage or moderate disease progression. This highlights the utility of the ApoE$^{-/-}$ model for studying the exacerbated effects of AS and the lipid metabolism and inflammatory pathways in more clinically relevant stages of the disease.

This study provides a comprehensive analysis of the interconnected processes of lipid metabolism, inflammation, plaque instability, and vascular remodeling in response to an HD. However, this study has several limitations. First, the present study focused solely on static measurements of key markers without addressing dynamic pathological changes or causal relationships between the observed factors. Second, while the ApoE$^{-/-}$ mouse model is valuable for studying AS, it may not fully replicate the complexity of human disease, necessitating cautious interpretation of the results [41]. Additionally, while KChIP2 expression was significantly upregulated in the coronary arteries of HD-fed mice, its mechanistic role in plaque instability remains unclear. Further research is needed to clarify whether KChIP2 contributes to plaque destabilization by modulating vascular smooth muscle cell behavior (e.g., contractility, proliferation) or promoting endothelial inflammation.

To address these limitations and strengthen the translational relevance of the findings, future studies should incorporate interventional approaches targeting key molecular markers, such as KChIP2, and employ more clinically relevant AS models. A more integrated investigation of the interplay between lipid metabolism, inflammation, plaque stability, and vascular remodeling will help clarify disease mechanisms and facilitate the development of targeted therapies for cardiovascular diseases.

Conclusion

This study demonstrated that an HD induces dyslipidemia, elevates inflammatory factors, increases the expression of plaque instability-related markers (such as PTX3, PLA2G7, and MMP-9), and exacerbates vascular fibrosis

and iron deposition. These findings highlight the critical role of HD in AS progression and provide valuable data to support further investigations into its underlying pathological mechanisms and to aid in the identification of potential therapeutic targets.

Availability of Data and Materials

The data used to support the findings of this study are available from the corresponding author upon request.

Author Contributions

WRW, YZQ, and PJH conceived and designed the study. WRW, YZQ, and PJH conducted the study. PJN, CC, YNC, and JL contributed to data acquisition. PJN, CC, YNC and JL analyzed the data. PJN, CC, YNC and JL interpreted the data. All authors contributed to the writing and critical revision of the manuscript and approved the final version. All authors have participated sufficiently in the work and agreed to be accountable for all aspects of the work.

Ethics Approval and Consent to Participate

This study was approved by the Medical Ethics Committee of The First Affiliated Hospital of Soochow University (SU-KY2215). Before the start of the experiment, all mice were adaptively fed with an ordinary diet for 1 week.

Acknowledgment

Not applicable.

Funding

This study was supported by Suzhou University Technology Cooperation Project (Number: H211064) and 2024 Suzhou University Affiliated First Hospital Boxi Clinical Research Key Project (Number: BXLC2024006).

Conflict of Interest

The authors declare no conflict of interest.

References

[1] Malekmohammad K, Bezsonov EE, Rafieian-Kopaei M. Role of Lipid Accumulation and Inflammation in Atherosclerosis: Focus on Molecular and Cellular Mechanisms. Frontiers in Cardiovascular Medicine. 2021; 8: 707529. https://doi.org/10.3389/fcvm.2021.707529.

[2] Lim Y, Jeong S, Hong M, Han HW. Non-Alcoholic Fatty Liver Disease, Atherosclerosis, and Cardiovascular Disease in Asia. Reviews in Cardiovascular Medicine. 2023; 24: 173. https://doi.org/10.31083/j.rcm2406173.

[3] Mehta A, Shapiro MD. Apolipoproteins in vascular biology and atherosclerotic disease. Nature Reviews. Cardiology. 2022; 19: 168–179. https://doi.org/10.1038/s41569-021-00613-5.

[4] Zhang S, Liu Y, Cao Y, Zhang S, Sun J, Wang Y, *et al*. Targeting the Microenvironment of Vulnerable Atherosclerotic Plaques: An Emerging Diagnosis and Therapy Strategy for Atherosclerosis. Advanced Materials (Deerfield Beach, Fla.). 2022; 34: e2110660. https://doi.org/10.1002/adma.202110660.

[5] Młynarska E, Czarnik W, Fularski P, Hajdys J, Majchrowicz G, Stabrawa M, *et al*. From Atherosclerotic Plaque to Myocardial Infarction-The Leading Cause of Coronary Artery Occlusion. International Journal of Molecular Sciences. 2024; 25: 7295. https://doi.org/10.3390/ijms25137295.

[6] Botros M, Fadah K, Mukherjee D. The role of inflammatory response in the development of atherosclerosis, myocardial infarction, and remodeling. Vessel Plus. 2024; 8: 31. https://doi.org/10.20517/2574-1209.2024.14.

[7] Lubrano V, Balzan S. Status of biomarkers for the identification of stable or vulnerable plaques in atherosclerosis. Clinical Science (London, England: 1979). 2021; 135: 1981–1997. https://doi.org/10.1042/CS20210417.

[8] Geng X, Liu H, Yuwen Q, Wang J, Zhang S, Zhang X, *et al*. Protective effects of zingerone on high cholesterol diet-induced atherosclerosis through lipid regulatory signaling pathway. Human & Experimental Toxicology. 2021; 40: 1732–1745. https://doi.org/10.1177/09603271211006170.

[9] Sinaga E, Suprihatin, Yenisbar, Iswahyudi M, Setyowati S, Prasasty VD. Effect of supplementation of Rhodomyrtus tomentosa fruit juice in preventing hypercholesterolemia and atherosclerosis development in rats fed with high fat high cholesterol diet. Biomedicine & Pharmacotherapy = Biomedecine & Pharmacotherapie. 2021; 142: 111996. https://doi.org/10.1016/j.biopha.2021.111996.

[10] Shinohata R, Shibakura M, Arao Y, Watanabe S, Hirohata S, Usui S. A high-fat/high-cholesterol diet, but not high-cholesterol alone, increases free cholesterol and apoE-rich HDL serum levels in rats and upregulates hepatic ABCA1 expression. Biochimie. 2022; 197: 49–58. https://doi.org/10.1016/j.biochi.2022.01.011.

[11] Kim D, Chung H, Lee JE, Kim J, Hwang J, Chung Y. Immunologic Aspects of Dyslipidemia: a Critical Regulator of Adaptive Immunity and Immune Disorders. Journal of Lipid and Atherosclerosis. 2021; 10: 184–201. https://doi.org/10.12997/jla.2021.10.2.184.

[12] Libby P. Inflammation during the life cycle of the atherosclerotic plaque. Cardiovascular Research. 2021; 117: 2525–2536. https://doi.org/10.1093/cvr/cvab303.

[13] El Zouka Y, Sheta E, Abdelrazek Salama M, Selima E, Refaat R, Salaheldin Abdelhamid Ibrahim S. Tetrandrine ameliorated atherosclerosis in vitamin D3/high cholesterol diet-challenged rats via modulation of miR-34a and Wnt5a/Ror2/ABCA1/NF-kB trajectory. Scientific Reports. 2024; 14: 21371. https://doi.org/10.1038/s41598-024-70872-y.

[14] Yang LG, March ZM, Stephenson RA, Narayan PS. Apolipoprotein E in lipid metabolism and neurodegenerative disease. Trends in Endocrinology and Metabolism: TEM. 2023; 34: 430–445. https://doi.org/10.1016/j.tem.2023.05.002.

[15] Bai Y, Feng Y, Jiang B, Yang Y, Pei Z, Yang Q, *et al*. The Role of Exercise in Reducing Hyperlipidemia-Induced Neuronal Damage in Apolipoprotein E-Deficient Mice. BioMed Research International. 2021; 2021: 5512518. https://doi.org/10.1155/2021/5512518.

[16] Ilyas I, Little PJ, Liu Z, Xu Y, Kamato D, Berk BC, *et al*. Mouse models of atherosclerosis in translational research. Trends in Pharmacological Sciences. 2022; 43: 920–939. https://doi.org/10.1016/j.tips.2022.06.009.

[17] Farooqui AA. Role of dyslipidemia in atherosclerosis. Stroke Revisited: Dyslipidemia in Stroke (pp. 3–14). Springer: Singapore. 2021. https://doi.org/10.1007/978-981-16-3923-4_1.

[18] Miao J, Zang X, Cui X, Zhang J. Autophagy, Hyperlipidemia, and Atherosclerosis. Advances in Experimental Medicine and Biology. 2020; 1207: 237–264. https://doi.org/10.1007/978-981-15-4272-5_18.

[19] Yang Y, Qu Y, Lv X, Zhao R, Yu J, Hu S, *et al*. Sesamol supplementation alleviates nonalcoholic steatohepatitis and atherosclerosis in high-fat, high carbohydrate and high-cholesterol diet-fed rats. Food & Function. 2021; 12: 9347–9359. https://doi.org/10.1039/d1fo01517f.

[20] Liang H, Jiang F, Cheng R, Luo Y, Wang J, Luo Z, *et al*. A high-fat diet and high-fat and high-cholesterol diet may affect glucose and lipid metabolism differentially through gut microbiota in mice. Experimental Animals. 2021; 70: 73–83. https://doi.org/10.1538/expanim.20-0094.

[21] Hu X, Liu Q, Guo X, Wang W, Yu B, Liang B, *et al*. The role of remnant cholesterol beyond low-density lipoprotein cholesterol in diabetes mellitus. Cardiovascular Diabetology. 2022; 21: 117. https://doi.org/10.1186/s12933-022-01554-0.

[22] Wu Z, Li X, Wen Q, Tao B, Qiu B, Zhang Q, *et al*. Serum LDL-C/HDL-C ratio and the risk of carotid plaques: a longitudinal study. BMC Cardiovascular Disorders. 2022; 22: 501. https://doi.org/10.1186/s12872-022-02942-w.

[23] Vekic J, Zeljkovic A, Cicero AFG, Janez A, Stoian AP, Sonmez A, *et al*. Atherosclerosis Development and Progression: The Role of Atherogenic Small, Dense LDL. Medicina (Kaunas, Lithuania). 2022; 58: 299. https://doi.org/10.3390/medicina58020299.

[24] Nesti L, Mengozzi A, Natali A. Statins, LDL Cholesterol Control, Cardiovascular Disease Prevention, and Atherosclerosis Progression: A Clinical Perspective. American Journal of Cardiovascular Drugs: Drugs, Devices, and other Interventions. 2020; 20: 405–412. https://doi.org/10.1007/s40256-019-00391-z.

[25] Gao M, Tang M, Ho W, Teng Y, Chen Q, Bu L, *et al*. Modulating Plaque Inflammation *via* Targeted mRNA Nanoparticles for the Treatment of Atherosclerosis. ACS Nano. 2023; 17: 17721–17739. https://doi.org/10.1021/acsnano.3c00958.

[26] Kong P, Cui ZY, Huang XF, Zhang DD, Guo RJ, Han M. Inflammation and atherosclerosis: signaling pathways and therapeutic intervention. Signal transduction and targeted therapy. 2022; 7: 131. https://doi.org/10.1038/s41392-022-00955-7.

[27] Lavin Plaza B, Phinikaridou A, Andia ME, Potter M, Lorrio S, Rashid I, *et al*. Sustained Focal Vascular Inflammation Accelerates Atherosclerosis in Remote Arteries. Arteriosclerosis, Thrombosis, and Vascular Biology. 2020; 40: 2159–2170. https://doi.org/10.1161/ATVBAHA.120.314387.

[28] Medrano-Bosch M, Simón-Codina B, Jiménez W, Edelman ER, Melgar-Lesmes P. Monocyte-endothelial cell interactions in vascular and tissue remodeling. Frontiers in Immunology. 2023; 14: 1196033. https://doi.org/10.3389/fimmu.2023.1196033.

[29] Pan J, Cai Y, Liu M, Li Z. Role of vascular smooth muscle cell phenotypic switching in plaque progression: A hybrid modeling study. Journal of Theoretical Biology. 2021; 526: 110794. https://doi.org/10.1016/j.jtbi.2021.110794.

[30] Olejarz W, Łacheta D, Kubiak-Tomaszewska G. Matrix Metalloproteinases as Biomarkers of Atherosclerotic Plaque Instability. International Journal of Molecular Sciences. 2020; 21: 3946. https://doi.org/10.3390/ijms21113946.

[31] Králíčková M, Laganà AS, Ghezzi F, Vetvicka V. Endometriosis and risk of ovarian cancer: what do we know? Archives of Gynecology and Obstetrics. 2020; 301: 1–10. https://doi.org/10.1007/s00404-019-05358-8.

[32] Poels K, Schnitzler JG, Waissi F, Levels JHM, Stroes ESG, Daemen MJAP, *et al*. Inhibition of PFKFB3 Hampers the Progression of Atherosclerosis and Promotes Plaque Stability. Frontiers in Cell and Developmental Biology. 2020; 8: 581641. https://doi.org/10.3389/fcell.2020.581641.

[33] Koay YC, Chen YC, Wali JA, Luk AWS, Li M, Doma H, *et al*. Plasma levels of trimethylamine-N-oxide can be increased with 'healthy' and 'unhealthy' diets and do not correlate with the extent of atherosclerosis but with plaque instability. Cardiovascular Research. 2021; 117: 435–449. https://doi.org/10.1093/cvr/cvaa094.

[34] Ye C, Zheng F, Wu N, Zhu GQ, Li XZ. Extracellular vesicles in vascular remodeling. Acta Pharmacologica Sinica. 2022; 43: 2191–2201. https://doi.org/10.1038/s41401-021-00846-7.

[35] Roldan LP, Roldan PC, Sibbitt WL, Jr, Qualls CR, Ratliff MD, Roldan CA. Aortic adventitial thickness as a marker of aortic atherosclerosis, vascular stiffness, and vessel remodeling in systemic lupus erythematosus. Clinical Rheumatology. 2021; 40: 1843–1852. https://doi.org/10.1007/s10067-020-05431-7.

[36] Farooq M, Hameed H, Dimanche-Boitrel MT, Piquet-Pellorce C, Samson M, Le Seyec J. Switching to Regular Diet Partially Resolves Liver Fibrosis Induced by High-Fat, High-Cholesterol Diet in Mice. Nutrients. 2022; 14: 386. https://doi.org/10.3390/nu14020386.

[37] Guo Q, Qian C, Qian ZM. Iron metabolism and atherosclerosis. Trends in Endocrinology and Metabolism: TEM. 2023; 34: 404–413. https://doi.org/10.1016/j.tem.2023.04.003.

[38] Meng H, Ruan J, Chen Y, Yan Z, Liu J, Wang X, *et al*. Trace Elements Open a New Direction for the Diagnosis of Atherosclerosis. Reviews in Cardiovascular Medicine. 2023; 24: 23. https://doi.org/10.31083/j.rcm2401023.

[39] Xu T, Cai J, Wang L, Xu L, Zhao H, Wang F, *et al*. Hormone replacement therapy for postmenopausal atherosclerosis is offset by late age iron deposition. eLife. 2023; 12: e80494. https://doi.org/10.7554/eLife.80494.

[40] Iacobas S, Amuzescu B, Iacobas DA. Transcriptomic uniqueness and commonality of the ion channels and transporters in the four heart chambers. Scientific Reports. 2021; 11: 2743. https://doi.org/10.1038/s41598-021-82383-1.

[41] Getz GS, Reardon CA. Do the Apoe-/- and Ldlr-/- Mice Yield the Same Insight on Atherogenesis? Arteriosclerosis, Thrombosis, and Vascular Biology. 2016; 36: 1734–1741. https://doi.org/10.1161/ATVBAHA.116.306874.